Journal of Low Temperature Physics, Vol. 54, Nos. 3/4, 1984

The Transverse Acoustic Impedance of He II*

M. J. Lea, P. Fozooni, and P. W. Retz†

Department of Physics, Bedford College, University of London, London, England

(Received July 29, 1983)

The complex shear acoustic impedance of liquid He II has been measured at frequencies $f(=\omega/2\pi)$ *of 20.5, 34.1, and 47.8 MHz from 30 mK to the* λ*-point* T_λ *(2.176 K). The impedance* Z *was found from the temperature dependence of the quality factor and the resonant frequency of a thickness shear mode quartz crystal resonator immersed in the liquid. The relationship for a hydrodynamic viscous liquid* $Z(T) = (1-i)(\pi f \eta \rho_n)^{1/2}$ *was used to measure the temperature dependence of the viscosity* $\eta(T)$ *using tabulated values of the normal fluid density* $\rho_n(T)$*. Deviations from hydrodynamic behavior occurred when the viscous penetration depth was less than the superfluid healing length, the phonon mean free path, and the roton mean free path. Near the* λ*-point,* $Z(T)/Z(T_\lambda)$ *was frequency dependent and a value for the superfluid healing length* $a = (0.10 \pm 0.01)\varepsilon^{-2/3}$ *nm was found, where* $\varepsilon = (T_\lambda - T)/T_\lambda$*. The effects of van der Waals forces near the crystal surface were also observed and a layer model was used to interpret the measurements. Below 1.8 K only rotons contribute significantly to* Z *and we determined the roton relaxation time as* $\tau_r = 8.5 \times 10^{-14} T^{-1/3} \exp(8.65/T)$ *sec. Below 1.2 K,* $\omega\tau_r > 1$ *and we investigated the breakdown of hydrodynamics in this region. For* $T < 0.6$ *K the resonant frequency of the crystals decreased by* $\Delta f/f = 2 \times 10^{-7}$*, but the origin of this effect is not yet known.*

1. INTRODUCTION

Ultrasonic techniques have been widely used to investigate the properties of condensed matter. In solids, both longitudinal and transverse sound polarizations are propagating modes. In a liquid the transverse mode is usually a strongly damped viscous wave whose properties can be determined from measurements of the complex shear specific acoustic impedance $Z = R - iX$.‡ We present here measurements of Z for superfluid ^{4}He at SVP

*Financial support provided by the SERC, Bedford College, and the Central Research Fund, University of London.

†Present address: Oxford Instruments Ltd., Osney Mead, Oxford, England.

‡For a time-dependent phase factor $e^{-i\omega t}$ as used here, the imaginary part of Z is negative. In electrical circuits it is more usual to use $e^{i\omega t}$, which changes the sign of the imaginary component in all expressions.

0022-2291/84/0200-0303$03.50/0

from 30 mK to the λ-point at frequencies $f\,(=\omega/2\pi)$ of 20.5, 34.1, and 47.8 MHz. Preliminary results have been published previously.[1]

From two-fluid hydrodynamics[2] Z is related to the viscosity η and the normal fluid density ρ_n by

$$Z = R - iX = (1-i)(\pi f \eta \rho_n)^{1/2} \tag{1}$$

Our experiments show that, while Eq. (1) is generally valid for He II, interesting deviations occur in three regions where the viscous penetration depth $\delta = (\eta/\pi f \rho_n)^{1/2}$ becomes smaller than the phonon mean free path, the roton mean free path, and the superfluid healing length, respectively.

The impedance Z was found from measurements of the temperature dependence of the quality factor $Q(T)$ and the series resonant frequency $f_s(T)$ of an AT-cut quartz crystal resonator immersed in He II. Similar measurements above 1.2 K have been performed by Yang[3] at 24 MHz, whose results, at rather high power levels, were strongly power dependent, and by Borovikov[4] at 25 MHz, who concluded that Eq. (1) was valid and could be used to determine η. Similar techniques have also been used to study liquid ^{3}He,[5] the superfluid film in a dilution refrigerator,[6] the onset of superfluidity in thin films of ^{4}He,[7] and of ^{3}He in ^{4}He,[8] and the properties of dilute mixtures of ^{3}He in ^{4}He.[9]

2. EXPERIMENTAL TECHNIQUES

2.1. Quartz Crystal Resonators

The resonators used in these experiments were thickness-shear mode AT-cut quartz crystals. These are commerically available but several were generously selected and donated by the GEC Hirst Research Centre, Wembley, London, England. The crystals were flat disks, of diameter 9.0 mm and thickness 0.25 mm, with 2.5×2.5 mm rectangular gold electrodes as shown in Fig. 1. The fundamental resonance was at 6.83 MHz, but for the thickness of gold plating used, 150 nm, this is not an energy-trapped mode,[10] and had a low Q value. For the third (20.5 MHz), fifth (34.1 MHz), and seventh (47.8 MHz) harmonics the acoustic energy is trapped by the electrodes and Q values greater than 10^5 were obtained. The gold plating, whose transversely vibrating surface interacts with the liquid helium, was very smooth, showing no structure on a scale of 10 nm as seen in an electron microscope. The crystals were used in their commercial mounting with two Be–Cu springs making contact with the electrodes via conducting epoxy resin.

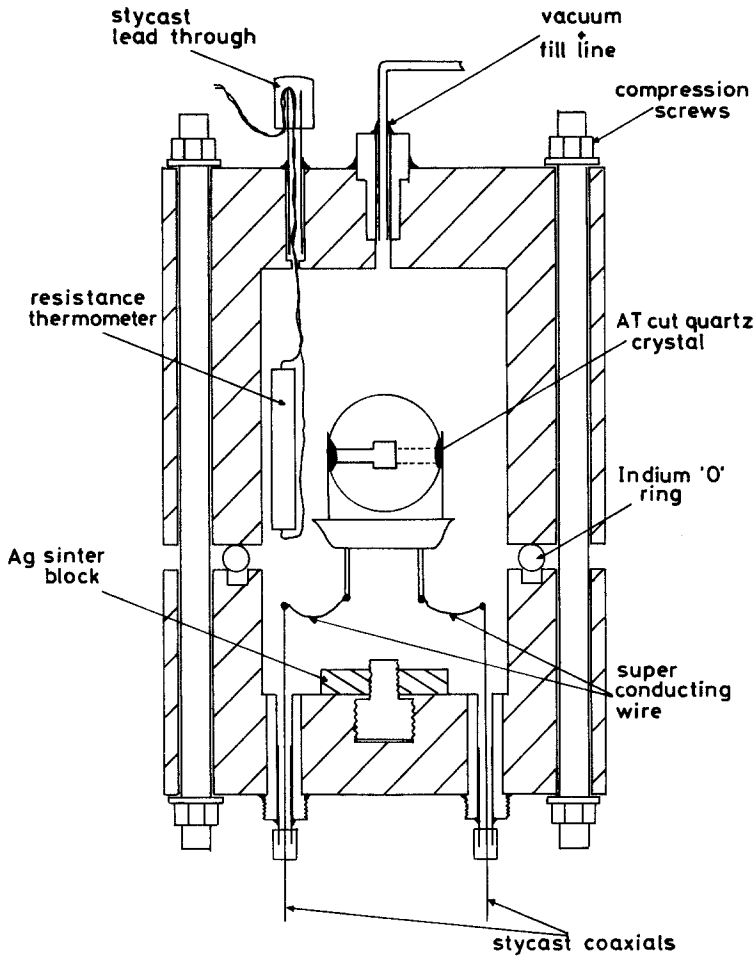

Fig. 1. The experimental cell used for the measurement of the transverse acoustic impedance of He II.

The resonant frequency and Q factor of the crystal were found using the transmission circuit shown in Fig. 2, in which the crystal was placed in series with a coaxial line connecting a 50-Ω cw transmitter (a Hewlett-Packard 8640B signal generator) and a 50-Ω receiver (a Miteq UA-4A-1210 low-noise preamplifier and a diode detector) whose dc output S was proportional to the transmitted rf power. A typical resonance curve at 20 MHz is shown in Fig. 3. The parameters measured during an experimental

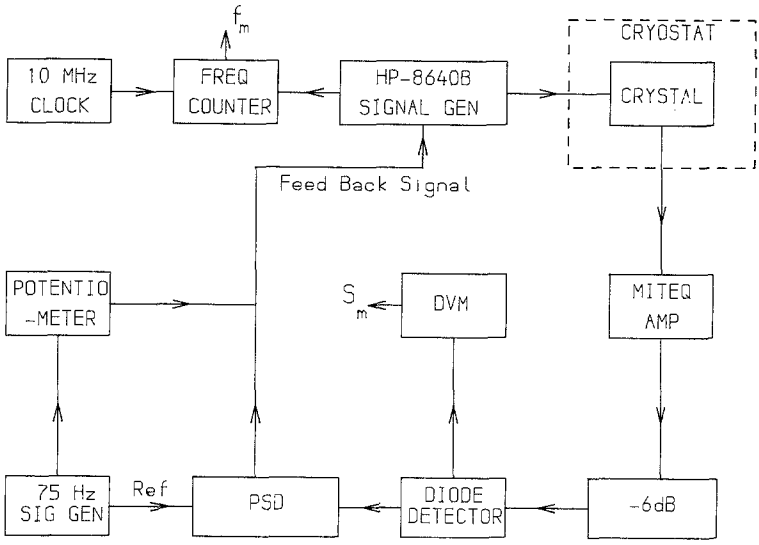

Fig. 2. Schematic block diagram of the feed back circuit used to lock on to a particular resonance of the quartz crystal.

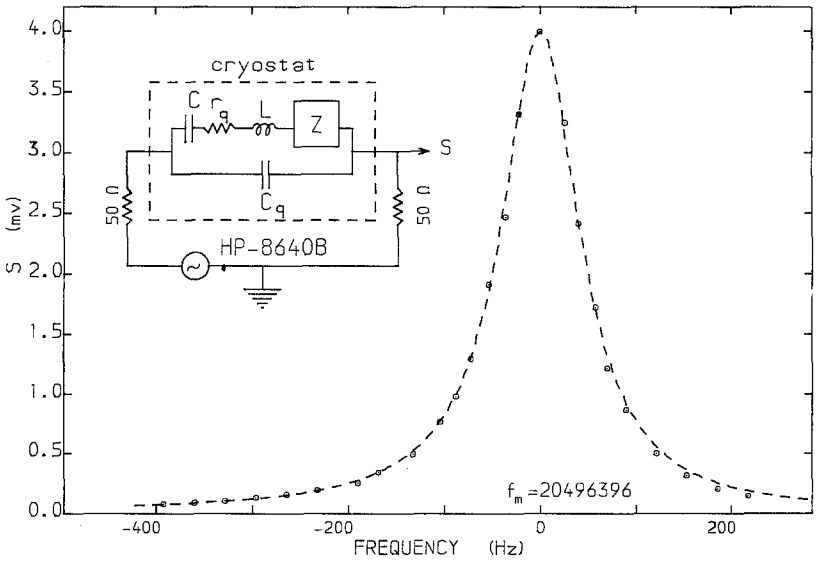

Fig. 3. The received signal S (O) as a function of frequency, showing the third harmonic resonance at 20.5 MHz of an AT-cut quartz crystal resonator immersed in liquid helium at 0.5 K. The line is the calculated response using the equivalent circuit shown. The Q of this crystal is 2.1×10^5.

run were the power $S_m(T)$ and frequency $f_m(T)$ of the maximum transmitted signal as functions of the temperature T. In order to relate these to the properties of the liquid helium in which the crystal was immersed we used the equivalent circuit[11,12] appropriate to an AT-cut crystal close to resonance as shown in Fig. 2. It consists of the static capacitance C_q ($=0.730\pm 0.006$ pF) of the crystal in parallel with the motional inductance L (≈ 0.18 H at 20 MHz), the motional capacitance C ($\approx 3.4\times 10^{-4}$ pF at 20 MHz), and a resistance r_q ($\approx 50\,\Omega$) that determines the intrinsic Q_q of the crystal. An ideal crystal ($r_q=0$) exhibits a series resonance at $f_s^0=1/2\pi(LC)^{1/2}$ and a parallel resonance (or antiresonance) at f_p^0, where $\Delta f_p=f_p^0-f_s^0\approx f_s^0 C/2C_q$ (≈ 4830 Hz at 20 MHz).

The effect of the liquid helium is to introduce an extra series electrical impedance $z=r-ix$, which is proportional to the transverse acoustic impedance of the helium $Z=R-iX$ and is temperature dependent. A figure of merit can be defined for the crystal in the helium as $M=(2\pi f C_q r_s)^{-1}$, where $r_s=r_q+r$ is the total series resistance of the equivalent circuit. At 20 MHz M varied from 210 to 50 as the temperature increased from below 0.5 K to the λ-point. For $M\gg 1$, C_q can be neglected to a first approximation and the total transmission system, including 50-Ω transmitter and receiver, behaved as a simple series resonant circuit with resonant frequency f_s and Q^{-1} given by

$$Q^{-1}=Q_q^{-1}+Q_c^{-1}+Q_{\mathrm{He}}^{-1}=(r_q+100+r)/\omega L=AS_m^{-1/2} \tag{2}$$

where the three contributions to Q^{-1} come from the crystal, the circuit, and the helium, respectively. Here A is a constant for the system and was determined directly from the transmission resonance curve in Fig. 3. Hence, during an experiment, Q^{-1} was found directly from S_m. The liquid helium decreases both Q and the resonant frequency by

$$Q_{\mathrm{He}}^{-1}=4R/n\pi R_q; \qquad \Delta f=f_s^0-f_s=2fX/n\pi R_q \tag{3}$$

where R_q is the transverse acoustic impedance of the quartz[13] ($R_q=8.862\times 10^6\,\mathrm{kg\,m^{-2}\,sec^{-1}}$, $\gg R, X$) and n is the harmonic number of the crystal resonance.

The effects of C_q are allowed for by applying circuit corrections to the measured values of S_m and f_m. First the frequency f_m of the maximum transmitted signal differs slightly from the series resonance frequency f_s (where the impedance of the $LCrz$ branch of the crystal equivalent circuit is real) by

$$f_m-f_s=-\Delta f_p(r_s+200)/M^2 r_s \tag{4}$$

and thus measurements of $f_m(T)$ were converted to $f_s(T)$. Also, S_m is larger than expected for the simple series circuit and the values were multiplied

by a correction factor

$$\alpha = 1 - 2(r_s + 200)/M^2(r_s + 100) \tag{5}$$

before Q^{-1} was calculated from Eq. (2). These corrections were small, particularly for S_m, but became significant at higher frequencies. The equivalent circuit used has been shown[14] to describe the response of these crystals over a wide frequency range, and the line in Fig. 3 shows the calculated response, which agrees well with the measured curves for that crystal.

In order to monitor $S_m(T)$ and $f_m(T)$ continuously a feedback circuit was used to "lock-on" to a particular crystal harmonic. A block diagram of the electronic system is shown in Fig. 2. The HP 8640B rf signal generator was frequency modulated at a low frequency of 75 Hz (less than the inverse decay time of the crystal f_s/Q) and the resultant small-amplitude modulation in the signal S was detected by a Brookdeal 9503 lock-in amplifier and phase sensitive detector (PSD), whose dc output changed sign as the rf frequency passed through f_m. This output was used to control the HP 8640B via the dc frequency modulation facility and thus lock-on to the frequency f_m of the maximum signal. The frequency resolution was then 0.1 Hz as measured on a Philips 9513 frequency meter. The magnitude of the frequency modulation could be made sufficiently small so to have negligible (<0.5%) effect on the values of S_m. An alternative system was also used, which phase-detected the rf transmitted signal and used the quadrature phase component (which changes sign at resonance) to lock the HP 8640B onto the resonance. The two systems produced identical results, but the first was preferred, as it was independent of any rf phase shifts in the system.

2.2. The Sonic Cell

The basic components of the sonic cell are shown schematically in Fig. 1. The cell body consisted of two sections of oxygen-free high-conductivity (OFHC) copper, which were sealed together with an indium O-ring. The crystal was held in its commercial mount and connected by short lengths of Niomax CN 61/05 superconducting wire to two coaxial feed throughs, which were sealed with Stycast 1266 epoxy resin. The rf signal was transmitted and received via two 50-Ω Cu/Ni coaxial lines[15] to room temperature. The cell was thermally anchored to the mixing chamber of an Oxford Instruments dilution refrigerator capable of reaching 15 mK. The coaxial lines, the ^{4}He capillary fill line, and all electrical leads were thermally anchored to the heat exchangers and mixing chamber of the dilution unit.

The experiments were performed by filling the cell with liquid ^{4}He until the crystal was covered but with the liquid surface within the cell at

all temperatures. Thermal contact between the liquid helium and cell body was achieved largely via a silver sinter block (supplied by Oxford Instruments, Oxford, England) and this gave a thermal relaxation time that was very small at high temperatures but rose to 1 sec at 50 mK. The heat leak directly into the liquid helium was measured to be 20 nW. The rf power dissipation in the crystal was typically 2 nW, giving a temperature differential between the crystal and the liquid helium estimated to be less than 0.3 mK at 0.1 K and less than 0.03 μK at 1 K.

The temperature was measured using 100-Ω, 1/2-W Speer resistors and 100-Ω, 1/8-W Allen-Bradley resistors as secondary thermometers to cover the range from 30 mK to 2.2 K. These resistors were calibrated against the vapor pressure of liquid ^{4}He, a CMN thermometer itself calibrated with an NBS SRM767 unit with superconducting fixed points at 1.180 K (Al), 0.851 K (Zn), and 0.519 K (Cd) and a ^{60}Co nuclear orientation thermometer below 50 mK. Checks for drift of the resistor calibration were made by comparison with a calibrated Ge thermometer. The λ-point of liquid He at 2.176 K was also used as a fixed point. All thermometry was done using the EPT-76 temperature scale.[16] The error in the temperature measurement is estimated to be less than 2% between 0.04 and 1 K and less than 1% above 1 K.

3. RESULTS

The procedure during an experiment was to cool the cell to 1 K, fill it with liquid ^{4}He, and then to lock on to a particular harmonic of the crystal and to measure $S_m(T)$ and $f_m(T)$ from 30 mK to the λ-point. The signal S_m increased dramatically below T_λ but became temperature independent below 0.6 K. The frequency f_m also increased below T_λ (by about 81, 105, and 125 Hz at 20.5, 34.1, and 47.8 MHz respectively), reaching a plateau near 0.5 K. It then decreased slightly (by only 3 Hz at 20.5 MHz) down to the lowest temperature reached. The circuit corrections were then applied to the data, using Eqs. (4) and (5). These corrections were maximum at the λ-point but were very small for S_m, being typically only 0.04, 0.18, and 0.44% at 20.5, 34.1, and 47.8 MHz respectively. The corrected values of $S_m(T)$ were then converted to values of $Q^{-1}(T)$, as plotted in Fig. 4, using the measured scaling factor A in Eq. (2). At 20.5 MHz the typical values of Q^{-1} at 0.5 K and T_λ were 6.1×10^{-6} and 1.30×10^{-5}, respectively. The circuit corrections to $f_m(T)$ were larger, particularly at the higher frequencies, being typically 2.9, 7.5, and 12.5 Hz at 20.5, 34.1, and 47.8 MHz, respectively, at T_λ. Hence values of $f_s(T)$ were obtained as plotted in Fig. 4.

The transverse acoustic impedance of He II should be zero at $T=0$, as the pure superfluid will exert no viscous drag or loading on the crystal.

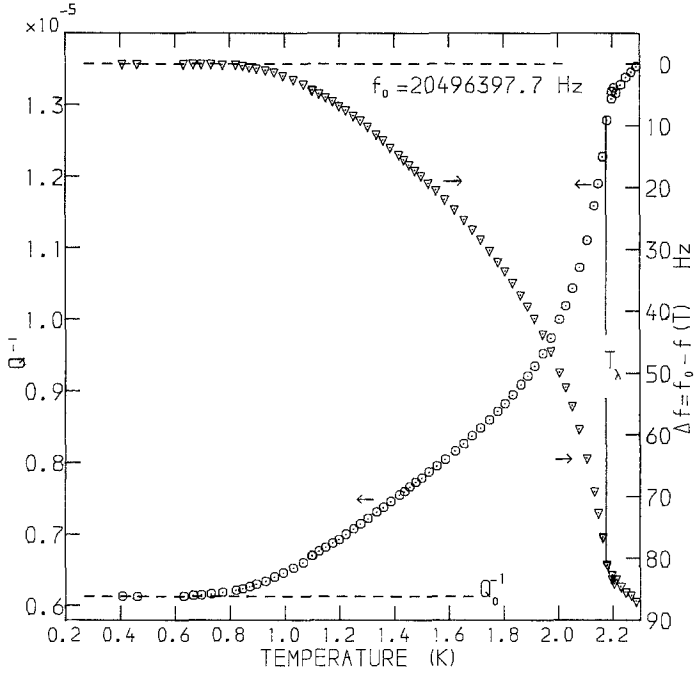

Fig. 4. Measurement of Q^{-1} and the frequency shift Δf at 20.5 MHz (third harmonic) of an AT-cut quartz crystal resonator immersed in liquid helium. The low-temperature limiting values Q_0^{-1} and f_0 are found from the data below 0.6 K.

This is confirmed by the temperature independence of Q^{-1} below 0.5 K, where $Q^{-1}(T<0.5\,\mathrm{K}) = Q_0^{-1}$, the residual value for the immersed crystal and circuit. $f_s(T)$ also increases to a limit f_0 below 0.5 K (for a discussion of the small decrease in f_s below 0.3 K, see section 4.4). We therefore ascribe the changes in Q^{-1} and f_s above 0.5 K to the effects of the liquid and we can use Eq. (3) to derive the real and imaginary parts of the transverse acoustic impedance of He II from

$$R(T) = [Q^{-1}(T) - Q_0^{-1}] n\pi R_q/4 \tag{6a}$$

$$X(T) = [f_0 - f_s(T)] n\pi R_q/2f_0 \tag{6b}$$

The values for R and X at 20.5, 34.1, and 47.8 MHz from 0.6 to 2.2 K are shown in Figs 5 and 6.

This analysis assumes that the baseline values of Q_0^{-1} and f_0 are themselves temperature independent above 0.5 K. In order to check this, an experiment was done with the cell evacuated. This is difficult since even very small amounts of ^{4}He, forming less than an atomic monolayer on the

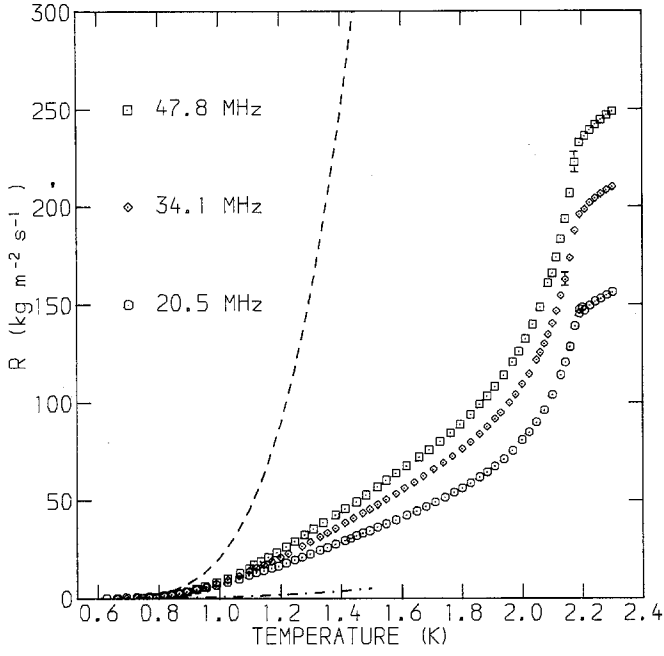

Fig. 5. Measurements of the real part R of the transverse acoustic impedance of He II at 20.5, 34.1, and 47.8 MHz. The upper line (- - -) shows the ballistic limit for rotons, Eq. (17) with $\alpha_r = 1$. The lower line (- · -) shows the ballistic limit for phonons, Eq. (11) with $\alpha_p = 1$.

crystal surface, can have dramatic effects on both Q^{-1} and the resonant frequency. However, in the cleanest cell we could achieve, the changes in Q^{-1} and f_s from 0.5 to 2.2 K were less than the experimental errors and we conclude that the crystal properties were temperature independent in this range. Mossuz and Gagnepain[17] have also investigated the temperature dependence of the resonant frequency of quartz crystals and found, at 4.2 K, $(1/f)\, df/dT \leq 4\times10^{-9}\,\mathrm{K}^{-1}$. Even if the frequency variation remained linear in T down to lower temperatures, the total frequency shift below T_λ at 20 MHz would be less than 0.2 Hz. However, it was noticed that Q^{-1} with no liquid present was typically 5.0×10^{-6}, slightly less than the value of 6.1×10^{-6} quoted above for Q_0^{-1}. Even the mechanical vacuum of He II has some effect on the residual losses of the crystal. The exact origin of the intrinsic Q^{-1} of these crystals is unknown, but a substantial part comes from the "leakage" of vibrational energy trapped beneath the electrodes into the periphery of the crystal.[10] Mode conversion could then generate longitudinal sound waves in the liquid. Also, if the resonance mode were not pure shear, then a longitudinal component of vibration could excite

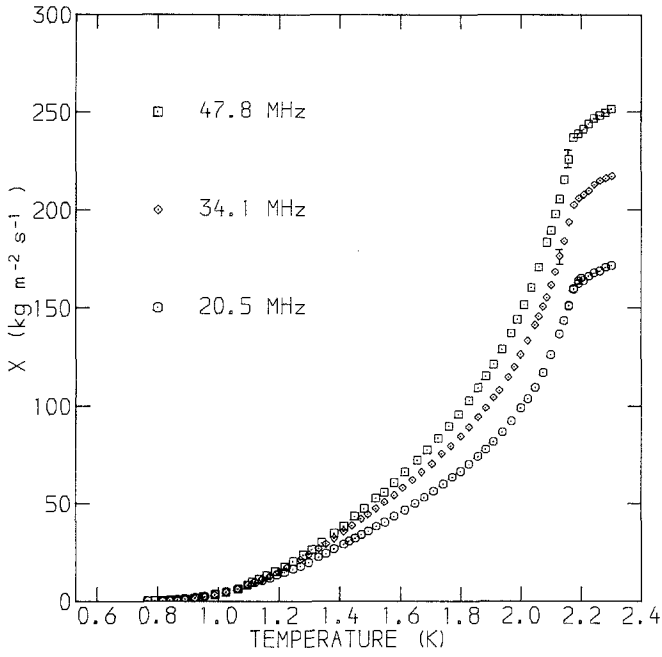

Fig. 6. Measurements of the imaginary part X of the transverse acoustic impedance of He II at 20.5, 34.1, and 47.8 MHz.

sound waves, though this effect should be very small. In either case a contribution to Q^{-1} would occur that was proportional to the longitudinal acoustic impedance ρu_1, where ρ is the total liquid density and u_1 is the speed of first sound. ρu_1 increases by only 7%[18] below T_λ and the resultant change in Q_0^{-1} would be less than 1% of the total contribution at T_λ from the transverse acoustic impedance, and therefore has been neglected.

The measurements reported here are at SVP and thus the pressure on the crystal will be temperature dependent, rising to 0.05 bar at the λ-point. We have measured the pressure coefficient of these crystals to be $(1/f)\, df/dP = 1.48 \times 10^{-6}$ bar^{-1}, which gives a total frequency change of 1.5 Hz at 20.5 MHz below T_λ. Consequently all the data in Fig. 6 have been corrected for the SVP variation. The quality factor Q_0 was found to be independent of pressure in this range.

The random errors in measuring Q^{-1} and f_s are estimated to be $\pm 1\%$ and ± 0.2 Hz, respectively. The errors in R and X at the λ-point are typically $\pm 2\%$, but the values of X are much more susceptible to systematic errors because of the corrections applied.

The rf power used to excite the crystal was normally -53 dBm, which gave a power dissipation in the crystal at the lowest temperatures of 2 nW,

similar to the power level used by Borovikov.[4] An increase in the power to −43 dBm produced no change in the results for R and X. This contrasts with the strong power dependence found by Yang[3] above 1.2 K at high power levels from 16 to 2500 μW.

4. ANALYSIS AND DISCUSSION

4.1. Effective Viscosity

As given in Eq. (1), the transverse acoustic impedance using the two-fluid model is

$$Z = (1-i)(\pi f \eta \rho_n)^{1/2} = R - iX$$

Since $\rho_n(T)$ is well known for He II we can use the values tabulated by Brooks and Donnelly[18] and Maynard[19] to define *effective viscosities* η_1 and η_2 from our measurements of R and X:

$$\eta_1(T) = R^2(T)/\pi f \rho_n(T); \qquad \eta_2(T) = X^2(T)/\pi f \rho_n(T) \tag{7}$$

(N.B.: η_1 and η_2 are *not* the real and imaginary parts of a complex dynamic viscosity. We quote values of η in cgs units poise, because of the universal use of this unit; the SI unit for dynamic viscosity is Pa sec, where 1 poise = 0.1 Pa sec). The effective viscosities derived from the 34.1-MHz data of Fig. 5 and 6 are plotted in Fig. 7 and show the features seen at all frequencies. Also shown in Fig. 7 are the values of the viscosity of He II as measured by Tough *et al.*[20] using a low-frequency vibrating wire viscometer. The value obtained at the λ-point for $\eta_1(T_\lambda)$ is 24.0 ± 0.4 μP, in reasonable agreement with the accepted value of 24.7 μP.[21] This shows that the quartz crystal is acting as a good *high-frequency viscometer.* The values of $\eta_2(T_\lambda)$ are rather larger, 27.5 ± 0.4 μP at 20.5 MHz, but we consider these to be less reliable as measurements of the viscosity both because of the corrections applied to X and because of other factors discussed below. Both η_1 and η_2 decrease rapidly below T_λ, as do the low-frequency measurements. Below 1.9 K, η_1 remains approximately constant, though exhibiting a small maximum, before decreasing rapidly below 1.2 K. The value of η_2 decreases steadily at all temperatures and is smaller than η_1 below 1.5 K. The low-frequency viscosity, however, has a minimum value near 1.5 K and increases exponentially at lower temperatures, a feature not seen in our data.

Vibrating wire viscometers measure the hydrodynamic viscosity, which below 1.8 K has been given by Khalatnikov[22] as a sum of the roton viscosity η_r and the phonon viscosity η_p,

$$\eta = \eta_r + \eta_p \tag{8}$$

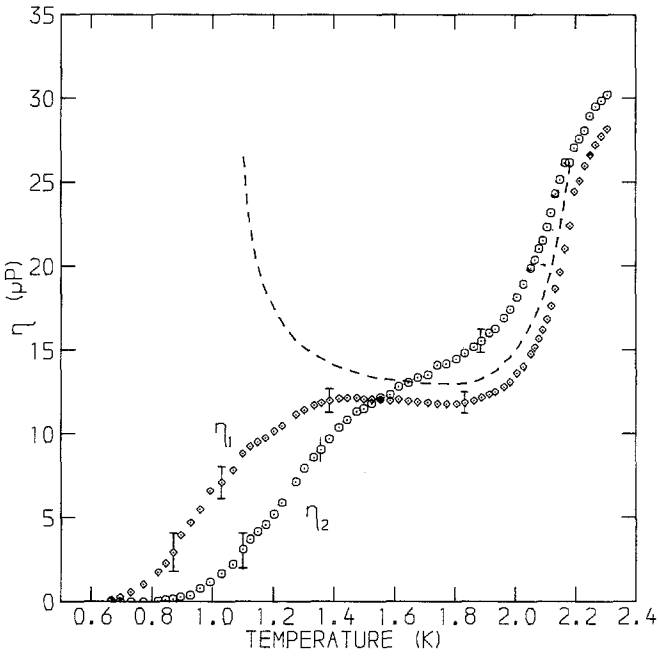

Fig. 7. The effective viscosities η_1 and η_2 as derived from the data for R and X at 34.1 MHz in Figs. 5 and 6, using Eq. (7). The line shows the hydrodynamic viscosity as measured with a vibrating wire viscometer, Ref. 20.

From 1.5 to 1.8 K, $\eta_r \gg \eta_p$ and is almost temperature independent (see Section 4.2). Below 1.5 K the phonon–roton scattering decreases exponentially and hence η_p increases. However, at 20 MHz and higher frequencies, the experimental conditions are often in the nonhydrodynamic region, where $\omega\tau > 1$, giving relaxation effects, and $l/\delta > 1$, giving nonlocal effects, where τ is a relaxation time and l is the mean free path of the excitations in the liquid. In this region the concept of viscosity and penetration depth become inappropriate, though the acoustic impedance Z, as seen by a quartz crystal resonator, remains well defined as

$$Z = \Pi/u \tag{9}$$

where Π is the shear stress on a surface whose tangential velocity is u, though the measurements of Z may be expressed as an effective viscosity. For a gas of excitations Z must be derived from the kinetic equation. For a single species of excitation Z is a function of $\omega\tau$, which also determines l/δ. In the collisionless, or ballistic, limit, when $\omega\tau \gg 1$ and $l/\delta \gg 1$, Π equals the transverse momentum flux away from the surface, and from simple

kinetic theory Eq. (9) becomes

$$Z_\infty = R_\infty = \alpha \rho_n \bar{c}/4; \qquad \omega\tau \gg 1 \tag{10}$$

where Z is then real and independent of f, ρ_n is the normal density of the excitations whose mean speed is $\bar{c}$, and α is the fraction of the excitations that are diffusely scattered at the surface (or absorbed and remitted). As $\omega\tau$ decreases, $R(\omega\tau)$ also decreases and in the hydrodynamic limit, $\omega\tau \ll 1$, Z must be given by Eq. (1). We know of no calculations of Z for a roton or phonon gas based on the Boltzmann equation similar to those for a Fermi gas or a Fermi liquid.[24]

In He II the situation is complicated by the presence of two types of interacting thermal excitations, phonons and rotons. For $T > 1.6\,\mathrm{K}$ our experiments are in the hydrodynamic regime, but η_p is then very small. At lower temperatures, the rapid rise in the hydrodynamic phonon viscosity has almost disappeared at 20 MHz, leaving only a very small peak in $\eta_1(T)$. Following Nadirashvili and Tsakadze,[25] we believe this is due to the large values of l_p/δ, where l_p is the phonon mean free path. They found that the effective phonon viscosity, as measured with a vibrating wire viscometer at 2150 Hz, was reduced from the hydrodynamic value for values of $l/\delta \approx 0.1$. For completely independent phonons and rotons we might expect two penetration depths, $\delta_r = (\eta_r/\pi f \rho_r)^{1/2}$ and $\delta_p = (\eta_p/\pi f \rho_p)^{1/2}$, where ρ_r and ρ_p are the normal fluid densities of rotons and phonons, respectively. But as the phonons are scattered mainly by the rotons above 0.9 K,[22] they will reach equilibrium with the rotons, with $\delta = \delta_r = (\eta_r/\pi f \rho_n)^{1/2}$ since $\rho_n \approx \rho_r \gg \rho_p$ above 1 K. Calculating the phonon mean free path from the theory of Khalatnikov,[22] we estimate that $l_p/\delta \approx 1.5$ at 1.6 K, rising to 35 at 1 K. Thus, at 1.8 K both phonons and rotons should be in the hydrodynamic region, but the phonons will make a negligible contribution to both η and Z. Below 1.5 K the phonons will enter the collisionless or ballistic region with an acoustic impedance given by

$$R_\infty = \alpha \rho_p u_{14} = 1.06 \alpha_p T^4 \,\mathrm{kg\,m^{-2}\,sec^{-1}} \tag{11}$$

The maximum collisionless limit ($\alpha_p = 1$) is plotted in Fig. 5, and is a small fraction of our measured values at all temperatures. If we interpret the small maximum in the effective viscosity η_1 as due to the phonon gas, then $\alpha_p \leq 0.3$ for phonon scattering at the smooth gold-plated crystal surface. The phonon contribution to our measured values of Z is therefore small and has been neglected in the discussion below.

4.2. Roton Viscosity

Below 1.9 K our experiments measure the effective roton viscosity. Figure 8 shows the effective viscosities η_1 and η_2 as measured as a function

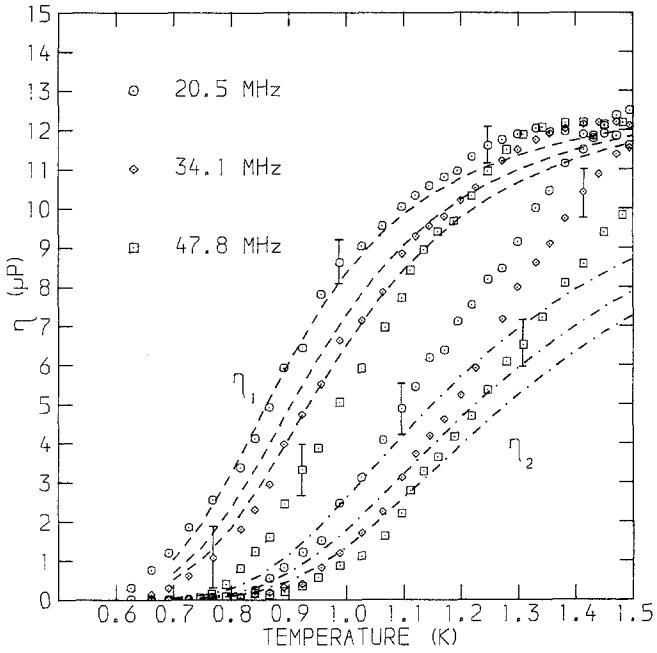

Fig. 8. The effective roton viscosities η_1 and η_2 at 20.5, 34.1, and 47.8 MHz from 0.6 to 1.5 K showing the breakdown of hydrodynamics. Theoretical calculations for η_1 (- - -) and η_2 (- · -) from Eq. (21) are shown for the three frequencies.

of temperature from 0.6 to 1.5 K at 20.5, 34.1, and 47.8 MHz. For simplicity, we have used the total normal fluid density in calculating the effective viscosity. If we use only the roton part of ρ_n in Eq. (7), then our values of $\eta(T)$ increase slightly but by less than the error bars at all temperatures. We identify the plateau region for η_1 between 1.2 and 1.5 K as giving the value of the hydrodynamic roton viscosity η_r, which has the value 12.5 ± 0.4 μP, in good agreement with other determinations based on the minimum in the hydrodynamic total viscosity[25,26] and the value of 11.8 μP deduced from capillary heat conduction measurements by Brewer and Edwards.[27,28]

The Landau–Khalatnikov[22] theory gives the roton viscosity as

$$\eta_r = p_0^2 N_r \tau_r / 15\mu \tag{12}$$

where N_r is the roton density and p_0 and μ are parameters of the roton dispersion relation $\mathscr{E}(p) = \Delta + (p - p_0)^2/2\mu$ as tabulated by Brooks and Donnelly.[18] Here τ_r is the relaxation time for the dominant roton–roton scattering, given by Khalatnikov[22] as

$$\tau_r^{-1} = 2p_0\mu |V_0|^2 N_r / \hbar^4 \tag{13}$$

where V_0 is a scattering pseudopotential. Hence η_r is temperature independent in this theory. There have been several later calculations,[29] particularly by Roberts and Donnelly,[28] who found

$$\tau_r^{-1} = \pi\Gamma(1/3)(2kT/\mu)^{1/2}(p_0^2/8\pi\rho kT)^{2/3}N_r \tag{14}$$

where $\Gamma(1/3) = 2.679$ and ρ is the total density. At SVP this gives $\eta_r = 10.9\ \mu$P at 1.5 K, lower than the measured value. This theory also predicts a weak temperature dependence $\eta_r \propto T^{1/6}$, but we are not able to distinguish between this and a temperature-independent roton viscosity, because of the temperature dependence of the roton parameters[18] and the error bars on our data.

Conversely, we can derive a relaxation time for roton–roton scattering from our data. If we take η_r as temperature independent, then we obtain

$$\tau_r^{-1} = (1.13 \pm 0.05) \times 10^{13} T^{1/2}\, e^{-\Delta/kT} \tag{15a}$$

where $\Delta = 8.65$ K.[18] If we assume the temperature dependence given by Eq. (14), then we find

$$\tau_r^{-1} = (1.18 \pm 0.05) \times 10^{13} T^{1/3}\, e^{-\Delta/kT} \tag{15b}$$

Below 1.2 K the effective roton viscosity decreases rapidly in the nonhydrodynamic region, where $\omega\tau_r > 1$ and $l_r/\delta > 1$, where l_r is the roton mean free path. For rotons $l_r = \tau_r \bar{v}_r$, where $\bar{v}_r$ is the mean roton velocity[30] $= (2kT/\pi\mu)^{1/2}$ [note that Roberts and Donnelly[28] use the classical expression $\bar{v}_r = (kT/\mu)^{1/2}$]. Since $\delta = (\pi f \eta \rho_n)^{1/2}$ and using Eq. (12) and the relation $\rho_r = N_r p_0^2/3kT$, we find that $l/\delta = (5\omega\tau_r/\pi)^{1/2}$. Thus the normalized effective viscosities η_1^* and η_2^* should be functions of $\omega\tau$,

$$\eta_1^* = \eta_1(\omega\tau)/\eta_r; \qquad \eta_2^* = \eta_2(\omega\tau)/\eta_r \tag{16}$$

where η_r is the hydrodynamic roton viscosity ($\omega\tau_r \ll 1$) at the same temperature. Figure 9 shows a plot of η_1^* versus $\omega\tau_r$ for the data in Fig. 8, assuming that $\eta_r \propto T^{1/6}$ and that τ_r is given by Eq. (15b). Note that the data for all three frequencies lie on a common curve, within the error bars. An almost identical plot is obtained if we assume that η_r is temperature independent and that τ_r is given by Eq. (15a).

Although there are no calculations of the transverse acoustic impedance of a roton gas in the nonhydrodynamic region, it is interesting to compare our data with some simple expressions. First, we can derive the collisionless limit ($\omega\tau_r \gg 1$) from Eq. (10) to find

$$Z_\infty = R_\infty = \alpha_r \rho_n \bar{v}_r/4 = 1.2 \times 10^5 \alpha_r\, e^{-\Delta/kT}\ \text{kg m}^{-2}\,\text{sec}^{-1} \tag{17}$$

which is independent of frequency and is plotted in Fig. 5 for diffuse scattering ($\alpha_r = 1$). The effect of finite $\omega\tau_r$ is to reduce the measured acoustic

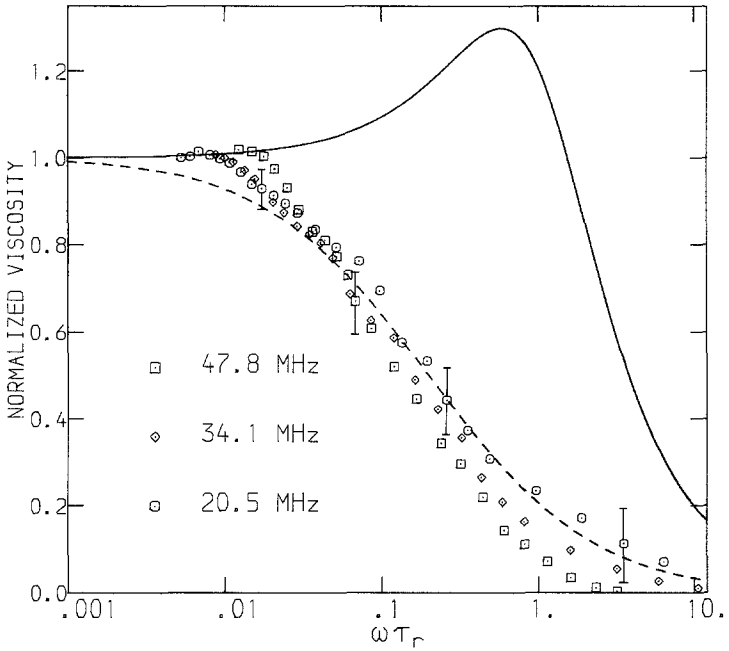

Fig. 9. The normalized viscosity η_1/η_r vs. $\omega\tau_r$ for the data in Fig. 8 assuming $\eta_r \propto T^{1/6}$ and $\tau_r = 8.5\times10^{-14}T^{-1/3}\exp(8.65/T)$. The lines are the functions η_1^* for a viscoelastic liquid, Eq. (19) (—), and from kinetic theory, Eq. (21) (- - -).

resistance R below this limit. Second, we can use the theory for a viscoelastic liquid,[31] which allows for relaxation effects only by substituting $\eta(\omega\tau) = \eta_r/(1-i\omega\tau)$ in Eq. (1) to obtain

$$Z(\omega\tau) = (1-i)[\pi f\rho_n\eta_r/(1-i\omega\tau)]^{1/2} \tag{18}$$

which gives

$$\eta_1^* = (x+\sqrt{x})/\omega\tau_r; \qquad \eta_2^* = (x-\sqrt{x})/\omega\tau_r \tag{19}$$

where $x = \omega^2\tau_r^2/(1+\omega^2\tau_r^2)$. The viscosity η_1^* for a viscoelastic liquid is plotted in Fig. 9 and shows a distinctive peak that is not seen in the data. Third, we can modify a kinetic theory expression derived by Borovikov and Peshkov,[6] which corrects the hydrodynamic impedance for finite values of l/δ:

$$Z(\omega\tau) = \frac{(1-i)(\pi f\eta_r\rho_n)^{1/2}}{1+(1-i)\beta l/\delta} \tag{20}$$

where $\delta = (\eta_r/\pi f\rho_n)^{1/2}$, and β is a numerical constant. This equation is strictly only valid as a correction to the hydrodynamic regime, but if we

choose $\beta = 2\pi/5\alpha_r$, then it reduces to the correct expressions both in the hydrodynamic ($\omega\tau \ll 1$) and collisionless ($\omega\tau \gg 1$) regions. In terms of η_1^* and η_2^* it gives

$$\eta_1^* = \left[\frac{1+2\beta l/\delta}{1+2\beta l/\delta+2(\beta l/\delta)^2}\right]^2$$
$$\eta_2^* = \left[\frac{1}{1+2\beta l/\delta+2(\beta l/\delta)^2}\right]^2 \tag{21}$$

where $l/\delta = (5\omega\tau_r/\pi)^{1/2}$. The viscosity η_1^* from Eq. (21) is plotted in Fig. 9 (we have assumed $\alpha_r = 1$) and is a reasonable fit to the data. The lines in Fig. 8 are the theoretical values given by Eq. (21) assuming that $\eta_r \propto T^{1/6}$ and that τ_r is given by Eq. (15b). The agreement with the measurements of η_1 is good at all temperatures, but the measured values of η_2 increasingly deviate from the theory as the temperature increases. We believe this is due to the effects of the healing length in He II (see Section 4.3), which has a strong influence on X (and hence η_2) but only a small effect on R (and hence η_1). Although Eq. (21) gives a good account of the roton viscosity in the nonhydrodynamic region, a correct theoretical treatment would enable a direct determination of τ_r to be made.

4.3. The Superfluid Healing Length

The analysis above assumes that the liquid helium that interacts with the vibrating crystal is homogeneous and has the same properties as the bulk liquid right up to the crystal surface. The viscous wave produced by the crystal has a viscous penetration depth $\delta = (\eta/\pi f\rho_n)^{1/2}$ that is only 16, 12, and 10 nm at 20.5, 34.1, and 47.8 MHz, respectively, at the λ-point. At lower temperatures δ increases, by a factor of 2.4 at 1.5 K, until the nonhydrodynamic region is entered. Any variation in the properties of He II over a scale comparable with δ will have an effect on our measurements. In particular, we expect the superfluid fraction to decrease to zero at an immersed solid surface. The healing length $a(T)$ is the characteristic distance over which the superfluid density $\rho_s(x)$, where x is the distance from the wall, reaches its bulk value $\rho_s(\infty) = \rho - \rho_n$. A solid wall has two main effects. First, the boundary condition for the superfluid order parameter at a plane wall at $x = 0$ is $\Psi(0) = 0$. From the Ginzburg–Pitaevskii–Mamaladze theory, Gross[32] and Sobyanin[33] have shown that the space dependence $\rho_s(x)$ is then given by

$$\rho_s(x) = \rho_s(\infty)\tanh^2(x/a) \tag{22}$$

where a is the healing length, which, on the general principal of scaling,[34]

is proportional to the phase correlation length $\xi(T)$. The constant of proportionality is not readily calculable from renormalization group theory,[34] but on the phenomenological Ginzburg–Pitaevskii–Mamaladze (GPM) theory[33] $a=\sqrt{2}\xi(T)$. Second, van der Waals forces between the wall (in our case, the gold electrodes) and the helium atoms produce an attractive potential of the form

$$U(x)/k=-\Phi/x^3=-1.986/x^3\,\mathrm{K} \tag{23}$$

where k is the Boltzmann constant, x is in nm, and the numerical value was measured by Chester and Yang[35,36] using similar gold-plated quartz crystals. This attraction increases the pressure and density of the helium near the wall.[36] A layer model is often used in which the first atomic layer is though to be solid helium with several statistical layers of liquid helium at enhanced pressure and density. For $T>1.7\,\mathrm{K}$ the pressure-dependent λ-line means that the high-pressure helium near the wall may be in the normal state.

The healing length can be defined as that thickness of a completely normal liquid helium layer next to the solid wall that would give the same excess mass of nonsuperfluid ^{4}He per unit area as observed experimentally. Thus the healing length, as measured in various experiments, may have contributions from four elements: the phase correlation length, a solid ^{4}He layer, a high-pressure normal liquid layer, and a high-pressure superfluid layer.

We can calculate the effects of these phenomena on our experiments by defining a local complex transverse acoustic impedance $Z_L(x)$, which is the impedance that a bulk homogeneous liquid would have with the same properties as exist locally at a distance x from the wall. The actual impedance at x, $Z(x)$, is found from transmission-line theory. By considering a small element of fluid at x it can shown[37,38] that

$$\frac{dZ(x)}{dx}=\gamma Z_L(x)\left[1-\frac{Z^2(x)}{Z_L^2(x)}\right]=i\rho_n(x)\omega\left[1-\frac{Z^2(x)}{Z_L^2(x)}\right] \tag{24}$$

where γ is the complex propagation constant for a wave of angular frequency ω in the fluid. For the special case of a local hydrodynamic viscous liquid with viscosity $\eta(x)$ and normal fluid density $\rho_n(x)$ Eq. (24) becomes

$$dZ(x)/dx=i\rho_n(x)\omega+Z^2(x)/\eta(x) \tag{25}$$

This first-order inhomogeneous differential equation is a Riccati equation and has no general analytic solution.[38] We have solved it for particular functions of $\eta(x)$ and $\rho_n(x)$ by numerical integration, using fourth-order Runge-Kutta techniques, from the boundary condition at $x=\infty$, $Z(\infty)=$

$(1-i)(\pi f\eta\rho_n)^{1/2}$, to obtain $Z(x)$ and, in particular, the liquid impedance seen by the crystal, $Z(0)$. For the special case of a thin homogeneous layer (thickness d, normal density ρ_L, impedance Z_L) between the crystal and bulk liquid (impedance Z_B), the incremental change in impedance from Z_B is

$$\Delta Z = -i\omega\rho_L d(1-Z_B^2/Z_L^2) \tag{26}$$

If the layer is a thin film in a vacuum ($Z_B = 0$), then

$$\Delta Z = -i\omega\rho_L d = -i\omega\sigma_L \tag{27}$$

where σ_L is the normal density per unit area of the film and the quartz crystal acts as a microbalance[7,8,35] with a frequency shift given by

$$\Delta f = -4f^2\sigma_L/nR_q \tag{28}$$

It can be seen from Eqs. (26) and (27) that the effect of thin ($d \ll \delta$) solid or liquid layers is primarily to change X and hence produce a frequency

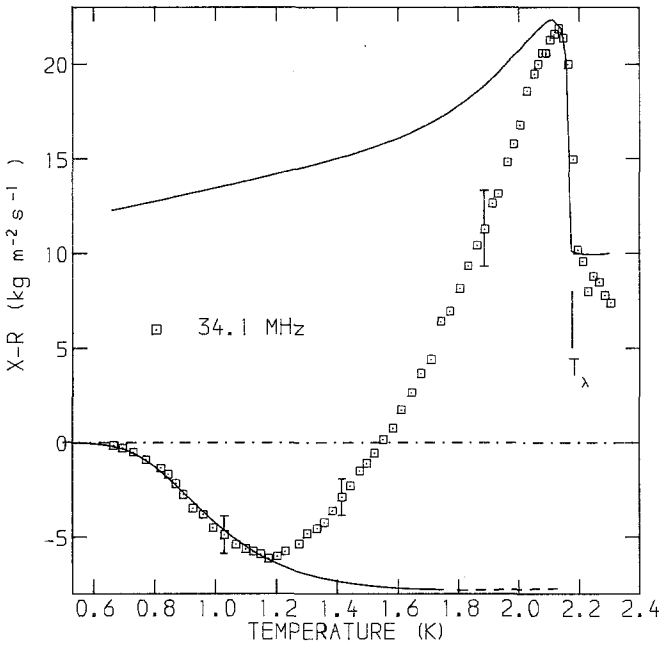

Fig. 10. Measurements of $\Delta X = X - R$ from the data at 34.1 MHz in Figs. 5 and 6. The lower line shows the expected behavior from the roton theory, Eq. (20), which is valid only below 1.8 K. The extraplo-ation of this theory is shown as a dashed line. The upper line shows the calculated ΔX for a superfluid healing length with $a = 0.10\varepsilon^{-2/3}$ nm near T_λ. This line has been placed to coincide with the data at the λ-point.

shift, Eq. (3), in a resonant crystal. Only very close to the λ-point ($\Delta T = T_\lambda - T < 2$ mK) should the healing length exceed δ, when ξ diverges as $\Delta T^{-2/3}$. Therefore, in analyzing our data it is appropriate to use $R(T)$ as a reference value and to look at the difference $\Delta X(T) = X(T) - R(T)$, which is plotted in Fig. 10 for the 34.1-MHz data shown in Figs. 4–7. Below 1.5 K, $\Delta X < 0$ in the nonhydrodynamic region of the roton viscosity as expressed in Eq. (20), which gives the values shown by the line in Fig. 10, tending to a limit for $\omega\tau_r \ll 1$:

$$\Delta X = -2\pi\beta f(10\eta_r\rho_n\tau/\pi)^{1/2} \propto -T^{-1/3} \tag{29}$$

This is shown as a dashed line above 1.8 K, where the concept of independent rotons is not valid.

However, ΔX deviates from the roton theory above 1.3 K and increases rapidly, becoming positive at 1.55 K and exhibiting a distinct peak below T_λ. We believe these effects are due to the healing length of He II and we shall first consider the region close to the λ-point.

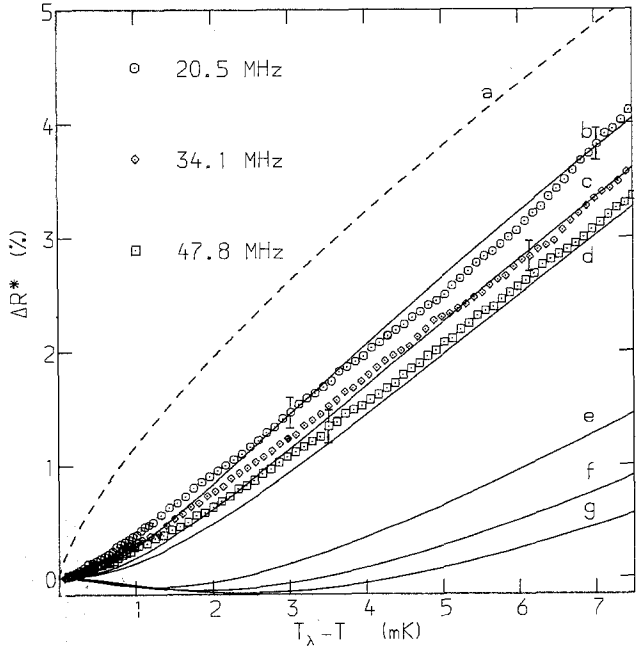

Fig. 11. Measurements of $\Delta R^* = R(T_\lambda) - R(T)/R(T_\lambda)$ vs. $\Delta T = T_\lambda - T$ at 20.5, 34.1, and 47.8 MHz. Line *a* shows the zero-frequency limit calculated from the measurements of Bruschi *et al.*[39] The lines *b*, *c*, *d* and *e*, *f*, *g* show the calculated temperature dependences for ΔR^* and ΔX^*, respectively, using Eq. (25) for 20.5 MHz (*b* and *e*), 34.1 MHz (*c* and *f*), 47.8 MHz (*d* and *g*).

Figure 11 shows measurements of the normalised acoustic resistance $R^* = R(T)/R(T_\lambda)$ at 20.5, 34.1, and 47.8 MHz just below the λ-point for $\Delta T < 7.5$ mK. These experiments were done using a chart recorder with the λ-point as a reference for both S_m and the temperature difference $\Delta T = T_\lambda - T$. The random error in these measurements relative to the λ-point was $\pm 0.1\%$ in R. Also shown are values of R^* derived using Eq. (1) from the precise measurements of η and ρ_n by Bruschi *et al.*[39] with a vibrating wire viscometer at 1792 Hz. If Eq. (1) were valid, then R^* should be independent of frequency. But the higher the frequency, the less sharp is the change in R^* at the λ-point. As f increases, the viscous wave samples an enhanced normal fluid density as δ becomes less than the healing length $a(T)$. For $\Delta T > 50$ mK the measurements of R^* coincide within experimental error at all frequencies, as $a(T)/\delta \ll 1$ in that region. To analyze these data we note that η/ρ_n and δ are much less temperature dependent than ρ_n or η. At 10 mK below T_λ, ρ_n has decreased by 6.6%, while δ has increased by only 0.7%. We therefore initially assume that $\eta(x, T) \propto \rho_n(x, T)$ and hence δ is independent of temperature and position x for the data in Fig. 11 and is equal to $\delta_\lambda(f)$, the value at the λ-point given above. At any temperature in Fig. 11 the effect of finite frequency is to reduce the

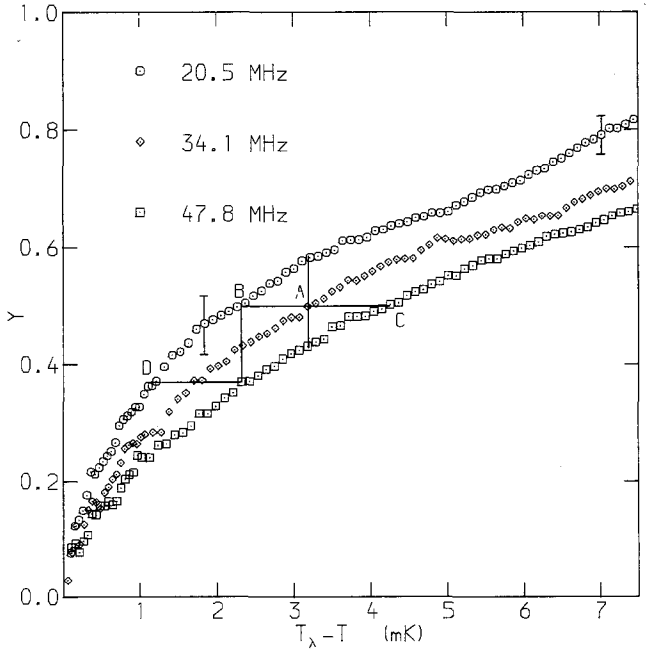

Fig. 12. Values of Y, Eq. (30), derived from the data shown in Fig. 11.

change in R^* and we define a frequency correction factor $Y(f, T)$, where

$$Y(f, T) = [1 - R^*(f, T)]/[1 - R^*(0, T)] = Y(a/\delta) \tag{30}$$

and we use the data of Bruschi *et al.*[39] to define $R^*(0, T) = [\eta(T)\rho_n(T)/\eta_\lambda\rho_\lambda]^{1/2}$, where η_λ and ρ_λ are the viscosity and density at the λ-point. The values of $Y(f, T)$ obtained from our data are shown in Fig. 12. As expected, Y tends to zero for ΔT small ($a \gg \delta$, the high-frequency limit) and to one for ΔT large ($a \ll \delta$, the low-frequency limit). For the special case of a healing length $a(T)$ that is a function of temperature only and a penetration depth δ that is a function of frequency only, then $Y(f, T)$ is a function only of the ratio a/δ, whose precise form depends on the superfluid density profile $\rho_s(x/a)$. [This conclusion was checked by numerical integration using Eq. (25)]. We can then deduce the temperature dependence of $a(T)$, except for a constant factor, as follows. At T_1 and frequency f_2 (point A in Fig. 12) the measured value of $Y(f_2, T_1)$ corresponds to an unknown value of $a(T_1) = K$, say. Then at T_2 (point B) we have $a(T_2) = (\delta_1/\delta_2)K$ since horizontal lines correspond to constant a/δ. Similarly, at T_3 (point C) we find $a(T_3) = (\delta_3/\delta_2)K$, while at T_4 (point D) we have $a(T_4) = (\delta_1^2/\delta_2\delta_3)K$ and so on. By analyzing the data at the three frequencies in this way, we derived the values of $a(T)$ shown in Fig. 13, which have a temperature dependence close to $\Delta T^{-2/3}$.

This critical exponent has been found in a number of experiments[21] and comes from the phase correlation length, which has been given by Halperin and Hohenburg[40] as

$$\xi(T) = m^2kT/4\pi\hbar^2\rho_s; \qquad \xi(T) = \xi_0\varepsilon^{-2/3} \quad \text{for} \quad \varepsilon \ll 1 \tag{31}$$

where m is the mass of a ^{4}He atom, and $\varepsilon = \Delta T/T_\lambda$. Near T_λ, $a(T)$ should be proportional to $\varepsilon^{-2/3}$ as observed experimentally. The absolute values of $a(T)$ shown in Fig. 13 were found by scaling the best fit line to $a = 0.10\varepsilon^{-2/3}$ nm, as explained below.

Having established the temperature dependence of $a(T)$, we can now develop the analysis beyond this phenomenological approach by numerically integrating Eq. (25) with the superfluid density profile given by Eq. (22), and hence

$$\rho_n(x) = \rho - \rho_s(x) = \rho + [\rho_n(\infty) - \rho]\tanh^2(x/a) \tag{32}$$

where the normal density at the crystal $\rho_n(0)$ is put equal to the total density ρ. We also assume that the local viscosity has the same functional form as $\rho_n(x)$

$$\eta(x) = \eta(0) + [\eta(\infty) - \eta(0)]\tanh^2(x/a) \tag{33}$$

where $\eta(\infty)$ is the bulk value in the superfluid and $\eta(0)$ is the local viscosity

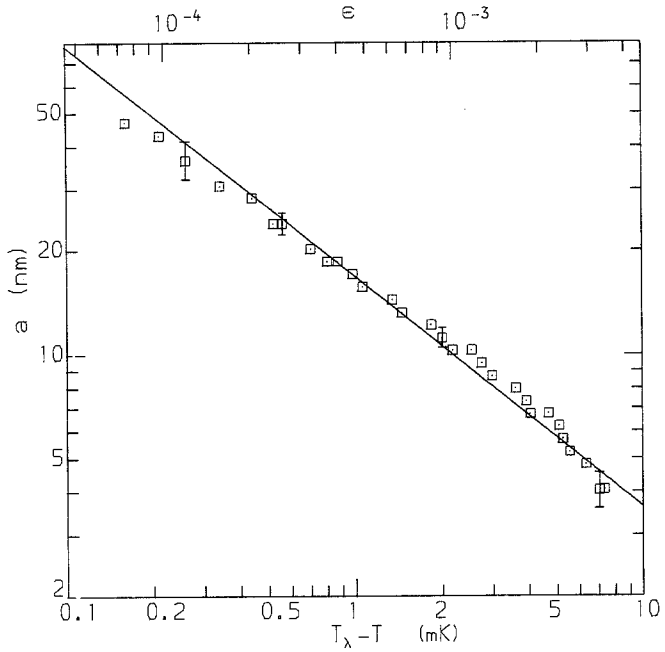

Fig. 13. Values of the superfluid healing length $a(T)$ obtained from Fig. 12 as described in the text. The line shows the best fit value $a = 0.10\varepsilon^{-2/3}$ nm.

in the normal layer at the crystal surface. Near T_λ, the temperature dependence of $\rho_n(\infty)$ and $\eta(\infty)$ are taken from the data of Bruschi *et al.*[39] The temperature dependence of $\eta(0)$ is not known below T_λ, so for these calculations we have assumed that $\eta(0) = \eta_\lambda$ and is temperature independent. This assumption is probably unrealistic, so we also performed the calculations with $\eta(0)$ proportional to T and to T^2. The results were almost identical close to T_λ and the differences at lower temperatures were small. We also assumed that $a(T)$ was proportional to $\xi(T)$, Eq. (31), and, near the λ-point, $a = a_0\varepsilon^{-2/3}$.

Having determined $\rho_n(x)$ and $\eta(x)$ we integrated Eq. (25) to find $Z(0)$, the measured impedance, for various values of a_0. The results for $R^*(f, T)$ are shown as lines in Fig. 11, with the overall best fit to our data being obtained for

$$a = (0.10 \pm 0.01)\varepsilon^{-2/3} \text{ nm} \tag{34}$$

The temperature dependence of X^* is also shown in Fig. 11 and, for $a/\delta > 1$, is quite different from the real part of the impedance. We were

not able to make such precise measurements of X^* close to T_λ. However, as shown in Fig. 10, a peak was seen in $\Delta X = X - R$ below T_λ whose magnitude was proportional to f. For $\Delta T > 50$ mK the real part of the normalized impedance R^* is essentially equal to the low-frequency limit. The calculations of ΔX at 34.1 MHz, with $a = 0.10$ nm, are shown in Fig. 10, using the right-hand scale, where $\Delta X = 0$ at the λ-point. ΔX increases almost discontinuously at T_λ to a maximum (proportional to f) near 2.1 K. The value of this jump in ΔX is proportional to a_0 and the good agreement with the data confirms that $a_0 = 0.10$ nm as deduced from the measurements of R.

As the temperature decreases, the healing length due to the phase correlation length, Eq. (31), becomes very small and is only 0.30 nm at 1.8 K, less than the thickness of a statistical monolayer of ^{4}He of 0.36 nm.[21] In this region the influence of the van der Waals forces should predominate. Close to the λ-point the potential, Eq. (23), might be expected to produce a layer of normal liquid of thickness d given by[33]

$$d = d_0 \varepsilon^{-1/3} = 0.29 \varepsilon^{-1/3} \text{ nm} \tag{35}$$

But Sobyanin[33] has shown that the combined effect of van der Waals forces and the phase correlation length is to produce a superfluid density profile of the form

$$\rho_s(x) = \rho_s(\infty) \tanh^2 [(x-b)/a] \tag{36}$$

where $a = \sqrt{2}\xi$ and

$$b = d^2/(a+d) = d_0^2/(a_0 + d_0 \varepsilon^{1/3}) \tag{37}$$

Very close to T_λ, as for the data in Fig. 11, b is temperature independent, $b \approx d_0^2/a_0 = 0.84 \text{ nm} \ll a$, and has negligible effect on our calculations for $\Delta T < 7.5$ mK. Some of this normal layer will be solid ^{4}He, which would produce only a temperature-independent frequency shift, Eq. (28), and not be detected in our experiments. Below 2.0 K, $b \approx d$ and the phase correlationlength can be neglected. The short range of the van der Waals forces means that the effect of the enhanced pressure and density near the crystal surface is to increase X, but not R, giving a finite value for ΔX even in He I, as seen in Fig. 10. The absolute value of ΔX above T_λ is uncertain because of the unknown extrapolation of the roton theory, Eq. (29), and the possibility of systematic errors in X between 0.5 and 2.2 K. Using the theory given by Oestereich and Stenschke,[36] we calculated the density and pressure $P(x)$ profiles [$P(x) \approx 6.1/x^3$ bar, where x is in nm] for the van der Waals potential in Eq. (23). From our measurements[41] of Z as a function of presure in He I we then derived $Z_L(x)$ just above T_λ. By numerically integrating Eq. (24) from the edge of the solid layer we estimated ΔX at

T_λ as 13 kg m^{-2} sec^{-1} at 34.1 MHz, which is comparable with the value found from the data in Fig. 10. In the superfluid state $Z_L(x)$ is strongly temperature dependent and difficult to estimate. To demonstrate the effects of the van der Waals forces we have calculated the impedance change that would be produced by a homogeneous viscous layer 1 nm thick with the properties of the bulk liquid at a pressure P between the quartz crystal and the He II at SVP. The local acoustic impedance $Z_L(T)$ in the layer was taken from our measurements of $R(T)$ for bulk ^{4}He at pressures of 6.7, 13.1, 20.3, and 24.8 bar.[42] The normal fluid density of the layer depends only on P and T and was taken from the tabulations by Brooks and Donnelly.[18] The results are shown in Fig. 14. Just below 2.176 K (T_λ at SVP) ΔX increases as Z_B decreases, while Z_L and ρ_L remain constant and the acoustic mismatch factor $(1-Z_B^2/Z_L^2)$ increases. When the layer itself becomes superfluid then both Z_L and ρ_L decrease, bringing ΔX down to zero at low temperatures. For a layer whose pressure was a smooth function of x the sharp transition would be rounded. Below 1.8 K the experimental temperature dependence of ΔX is close to that of a 0.6-nm layer at 24.8 bar (or a thicker layer at a lower pressure). However, it must be stressed that

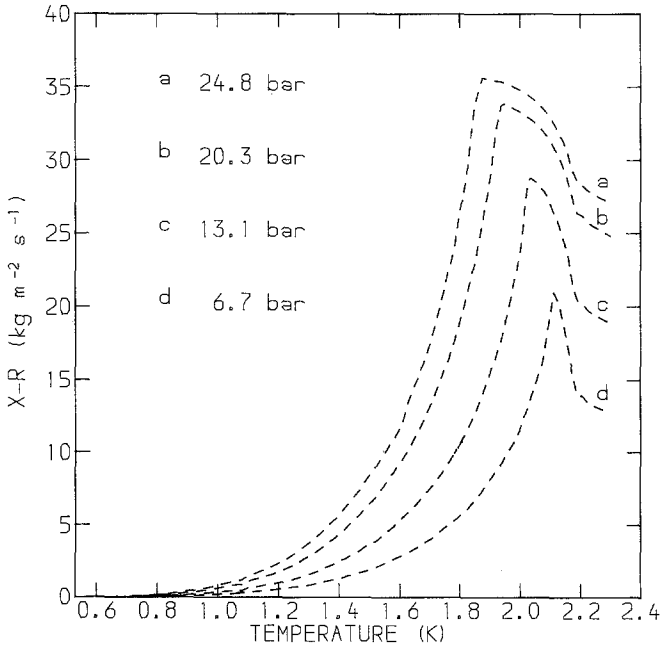

Fig. 14. Calculations of the impedance increment $\Delta X = X - R$ produced by a 1-nm layer of viscous liquid helium at pressures of 6.7, 13.1, 20.3, and 24.8 bar between the quartz crystal and the bulk ^{4}He at SVP.

the calculations treat the liquid helium as a continuum on a distance scale comparable with the atomic dimensions of ^{4}He.

4.4. Below 0.6 K

At temperatures below 0.6 K the ballistic loss of energy from the quartz crystal into the roton and phonon gases is negligible and the crystal is in a mechanical vacuum of He II. As expected, $Q(T)$ was temperature independent in this region. But in all our experiments, with three separate crystals, the resonant frequency $f(T)$ decreased again below 0.5 K, as shown in Fig. 15 for the third, fifth, and seventh harmonics. The fractional frequency shift was very small ($\Delta f/f < 2\times 10^{-7}$) even compared with the effects of viscous loading and was the same for all harmonics. Our initial interpretation[1] was that it was due to the thermal mobilization of a layer of ^{4}He atoms on the crystal surface at low temperatures, giving a frequency shift through the microbalance equation (28),

$$\Delta f/f = -4(f/n)\sigma(T)/R_q \tag{38}$$

where $\sigma(T)$ is a temperature-dependent areal mass density. The data below

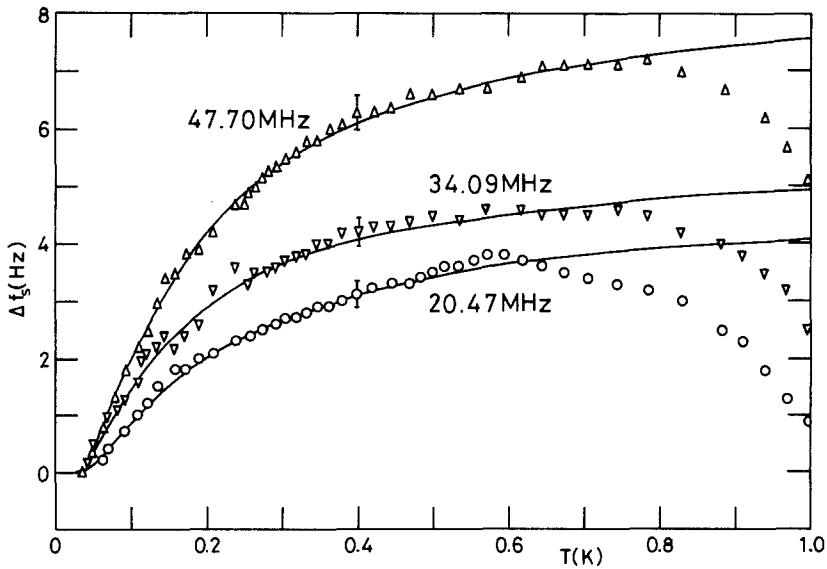

Fig. 15. Measurements of the frequency shift below 0.6 K of a quartz crystal resonator in He II at the third (20.5 MHz), fifth (34.1 MHz), and seventh (47.8 MHz) harmonics. The solid lines show the fits to the data using Eqs. (38) and (39).

0.6 K are well described by

$$\sigma(T) = \sigma(0)[1 - \exp(-\Theta/kT] \tag{39}$$

where $\Theta = 0.15 \pm 0.01$ K and $\sigma(0) = (6.3 \pm 0.4) \times 10^{-8}$ kg m^{-2}, which is comparable with the areal density of 5.3×10^{-8} kg m^{-2} of a statistical monolayer of ^{4}He atoms at normal fluid density. In order to confirm that this effect was due to ^{4}He, a run was performed with the cell evacuated and the crystal thermally anchored through the mounting. The effects in a vacuum (and also in low-pressure ^{3}He and ^{4}He gases) were complex and not very reproducible. The frequency and Q were temperature independent down to 0.5 K, but at lower temperatures, particularly near 0.2 K, both positive and negative frequency shifts occurred of the same order of magnitude as those shown in Fig. 15. These shifts depended on the thermal history of the crystal and could be changed by a burst of high power (1 mW) at 4.2 K or by thermal cycling. This suggests the effects were associated with the surface of the crystal though no helium could be detected in the cell with a mass spectrometer. However, since even a submonolayer of ^{4}He selectively adsorbed onto the crystal could undergo various transitions,[43] the presence of an otherwise undetectable quantity of ^{4}He cannot be ruled out. When liquid ^{4}He was subsequently admitted to the cell the results again became reproducible.

The origin of these effects has not yet been determined, but certainly these crystals are very sensitive to small amounts of both ^{4}He and ^{3}He.

5. CONCLUSIONS

In this paper we have presented measurements of the properties of liquid ^{4}He using a quartz resonator immersed in the liquid. In the hydrodynamic region the crystal acts as a high-frequency viscometer and measurements of the transverse acoustic impedance, particularly the real part, can be used to determine the temperature-dependent viscosity $\eta(T)$. Below 1.9 K only the roton viscosity is measured, the contribution from the phonons being small. Below 1.2 K the transition from hydrodynamic to nonhydrodynamic behavior was observed as l/δ and $\omega\tau > 1$. We point out the need for a correct theoretical treatment of the transverse acoustic impedance of a roton gas.

The transverse acoustic impedance is also sensitive to the inhomogeneity of the liquid helium produced by the solid crystal surface. Measurements close to the λ-point give a value for the healing length $a(T) = 0.10\varepsilon^{-2/3}$ nm, which has the same temperature dependence as, and is comparable in magnitude to, other characteristic lengths determined from

measurements on thin films in confined geometries or of ultrasonic attenuation.[21] However, we believe that our result is a good estimate of the healing length produced by the phase correlation length alone since, near T_λ, $\xi(T)$ is much larger than the range of the van der Waals forces. Also, the geometry in our experiments, a plane solid surface, is ideal. If we accept that $a = \sqrt{2}\xi$, as on the GPM theory, then a theoretical value for $a_0 = 0.038$ nm can be found from Eq. (31), but as pointed out by Hohenberg *et al.*[34] the choice of the numerical constant in Eq. (31) is conventional and ξ_0 may be larger by a factor of 4π!

Between 1.3 and 2.0 K the healing length is dominated by the van der Waals forces, which produce enhanced pressure and density within a few nanometers of the crystal surface. This layer increases the imaginary part of the transverse acoustic impedance and below 1.8 K is equivalent to a thin layer of thickness 0.6 nm at a pressure of 24.8 bar.

Below 0.6 K the frequency of the crystal resonantors decreased by a small amount, comparable with the shift produced by the freezing of one monolayer of ^{4}He atoms, but no clear interpretation has been found.

ACKNOWLEDGMENTS

We would like to thank Prof. E. R. Dobbs for his constant encouragement and support; Dr. E. Read and A. Dyer of the GEC Hirst Research Centre for supplying the quartz crystals; A. K. Betts, F. Greenough, A. King, F. Grimes, and others for technical assistance; and the Guernsey Education Council for a Research Studentship (for PWR).

REFERENCES

1. M. J. Lea and P. W. Retz, *Physica* **107B**, 223 (1981).
2. S. J. Putterman, *Superfluid Hydrodynamics* (North-Holland, Amsterdam, 1974).
3. L. C. Yang, Ph.D. Thesis, University of California at Los Angeles (1973).
4. A. P. Borovikov, *Prib. Tekh. Eksp.* **19**, 184 (1976) (*Instrum. Expt. Tech. (USSR)* **19**, 223 (1976).
5. P. R. Roach and J. B. Ketterson, *Phys. Rev. Lett.* **36**, 736 (1976); *J. Low Temp. Phys.* **25**, 637 (1976).
6. A. P. Borovikov and V. P. Peshkov, *Zh. Eksp. Teor. Fiz.* **70**, 300 (1976) [*Sov. Phys.-JETP* **43**, 156 (1976)].
7. L. C. Yang and P. V. Mason, *Cryogenics* **20**, 91 (1980); J. A. Herb and J. G. Dash, *Phys. Rev. Lett.* **35**, 171 (1975), and references therein.
8. E. Webster, G. Webster, and M. Chester, *Phys. Rev. Lett.* **42**, 243 (1979).
9. M. J. Lea and P. W. Retz, *Physica* **107B**, 225 (1981).
10. J. F. Werner and A. J. Dyer, in *Proceedings of the 30th Annual Symposium on Frequency Control*, (1976), p. 40.
11. D. A. Berlincourt, D. R. Curran, and H. Jaffe, *Physical Acoustics*, Vol. 1A, W. P. Mason and R. N. Thurston, eds. (Academic Press, New York, 1964), p. 169.

12. D. Firth, Quartz Crystal Oscillator Circuit Design Handbook, Department of the U. S. Army, Project No. 3A99-15-004 (1965).
13. H. J. McSkimin, P. Andreatch, and R. N. Thurston, *J. Appl. Phys.* **36**, 1624 (1965).
14. R. M. Peach, private communication.
15. D. P. Almond and M. J. Lea, *Cryogenics* **14**, 25 (1974).
16. M. Durieux, W. R. G. Kemp, C. A. Swenson, and D. N. Astrov, *Metrologia* **15**, 65 (1979).
17. G. Mossuz and J. J. Gagnepain, *Cryogenics* **16**, 652 (1976).
18. J. S. Brooks and R. J. Donnelly, *J. Phys. Chem. Ref. Data* **6**, 51 (1977).
19. J. Maynard, *Phys. Rev. B* **14**, 3868 (1976).
20. J. T. Tough, W. P. McCormick, and J. G. Dash, *Phys. Rev.* **132**, 2373 (1963).
21. G. Ahlers, in *The Physics of Liquid and Solid Helium*, K. H. Bennemann and J. B. Ketterson, eds. (Wiley, New York, 1976), Vol. I, Chapter 2, p. 85.
22. I. M. Khalatnikov, in *The Physics of Liquid and Solid Helium*, K. H. Bennemann and J. B. Ketterson, eds. (Wiley, New York, 1976), Vol I, Chapter 1, p. 1.
23. E. H. Kennard, *Kinetic Theory of Gases* (McGraw-Hill, New York, 1938).
24. P. W. Retz and M. J. Lea, *J. Phys. C* **15**, L207 (1982); R. W. Richardson, *Phys. Rev. B* **18**, 6122 (1978).
25. Z. Sh. Nadirashvili and Dzh G. Tsakadze, *J. Low Temp. Phys.* **37**, 169 (1979); *Sov. J. Low Temp. Phys.* **4**, 711 (1978).
26. J. Wilks, *Liquid and Solid Helium* (Clarendon Press, Oxford, 1967).
27. D. F. Brewer and D. O. Edwards, in *Proceedings of the 8th International Conference on Low Temperature Physics*, Davies ed. (Butterworths, 1963), p. 96.
28. P. H. Roberts and R. J. Donnelly, *J. Low Temp. Phys.* **15**, 1 (1974).
29. T. Sugiyama, *Progr. Theor. Phys.* **63**, 1170 (1980), and references therein.
30. I. M. Khalatnikov, *Usp. Fiz. Nauk* **59**, 673 (1956).
31. T. A. Litovitz and C. M. Davis, *Physical Acoustics*, Vol. IIA, W. P. Mason, ed. (Academic Press, New York, 1965), p. 281.
32. E. P. Gross, *J. Math. Phys.* **4**, 195 (1963).
33. A. A. Sobyanin, *Sov. Phys.-JETP* **36**, 941 (1973).
34. P. C. Hohenburg, A. Aharony, B. I. Halperin, and E. D. Siggia, *Phys. Rev. B* **13**, 2986 (1978).
35. M. Chester and L. C. Yang, *Phys. Rev. Lett.* **31**, 1377 (1973).
36. T. Oestereich and H. Stenschke, *Phys. Rev. B* **16**, 1996 (1977).
37. M. J. Lea, P. Fozooni, and P. W. Retz, to be published (1983).
38. R. A. Waldron, *Theory of Guided Electromagnetic Waves* (Van Nostrand Reinhold, London, 1969), p. 67.
39. L. Bruschi, G. Mazzi, M. Santini, and G. Torzo, *J. Low Temp. Phys.* **18**, 487 (1975).
40. B. I. Halperin and P. C. Hohenburg, *Phys. Rev.* **177**, 952 (1969).
41. M. J. Lea and P. Fozooni, to be published.
42. M. J. Lea and P. Fozooni, *Phys. Lett.* **93A**, 91 (1982).
43. J. G. Dash, *Films on Solid Surfaces* (Academic Press, London, 1975).